Multistep Reaction Model for Ignition of Nanocomposite Thermites

R.A. Williams, M. Schoenitz, A. Ermoline and E. L. Dreizin

MCAPN–2014–2a

Keywords: Nanocomposite thermites, micro-calorimetry, arrested reactive milling (ARM), reaction kinetics

ABSTRACT

Nanocomposite thermites include a reactive metal, in most cases aluminum, mixed on the nano-scale with a metal oxide. The nano-scale mixing achieved by ball-milling produces a highly developed and unusual interface area between reactive components. The high interface area assures a high reaction rate, attractive for propellants, explosives, and pyrotechnics. Development of a kinetic model for the initiation mechanisms of nanocomposite thermites prepared by arrested reactive milling (ARM) relies on differential scanning calorimetry (DSC) and thermal gravimetry (TG). These measurements identify and characterize multiple reaction steps important for ignition of these materials. However, for the ARM-prepared nanocomposites, interpretation of the DSC/TG data is challenging because of substantial but poorly resolved exothermic reactions occurring at low temperatures. These low temperature reactions are expected to contribute significantly to the processes that lead to ignition. Here, DSC and TG measurements were complemented by isothermal micro-calorimetry using TAM III resolving and quantifying these low temperature reactions. Based on the TAM III results, the accelerated oxidation in the ARM-prepared nano-thermites at low temperatures was attributed to Cabrera-Mott reaction, where the growth of very thin oxide layers is accelerated by electric field induced across such layers. This enabled a reaction mechanism for a 2Al·3CuO nanocomposite powder prepared by ARM to be developed that included multiple oxidation steps starting with the CM reaction followed by direct oxidative growth of and phase changes in different alumina polymorphs.

INTRODUCTION

Nanocomposite aluminum-based reactive materials may be used as additives to or main components of propellants, explosives, and pyrotechnics [1, 2]. Fully-dense nanocomposite powders prepared by Arrested Reactive Milling (ARM) [3-6] support high reaction rates associated with nano-scale mixing of reactive components, while offering relative simplicity of handling and mixing of conventional micron-sized powders.

Low temperature exothermic reactions may contribute significantly to the processes that lead to ignition of nanocomposite thermites [7-9]. A mechanism for aluminum-based materials accounts for polymorphic phase changes in the growing alumina layer [10], similar to aluminum oxidation in gaseous oxidizers [11]. However, the onset of low-temperature redox reactions in the ARM-prepared thermites occurs earlier than for Al oxidation in gas oxidizers [12-14]. Our recent experiments employing TAM III by TA Instruments [8] quantified exothermic reactions occurring at 303-373 K. Understanding and quantitative description of such reactions is necessary to model ignition in such nanocomposite materials.

For very thin oxide layers separating metal from gaseous oxidizers, oxidation is described using Cabrera-Mott (CM) model [15-16], in which mass transfer is accelerated by electric fields formed across the growing oxide films. This model may also describe reactions in condensed heterogeneous systems [17]. Here, the kinetics of the ARM-prepared Al-CuO thermites is studied and interpreted using low-temperature micro-calorimetry and previous differential scanning calorimetry (DSC) measurements [12].

EXPERIMENTAL

A stoichiometric, fully-dense 2Al•3CuO nanocomposite powder was prepared by mechanical milling powders of Al and CuO in Ar using hexane as a process control agent [12]. The heat release in the nanocomposite thermite was studied using TAM III under isothermal conditions at 303 - 413 K.

The results of TAM III measurements are shown in Fig. 1. The reaction rates are increasing with temperature. For a freshly prepared sample, even at a relatively low temperature of 303 K, a quantifiable heat release is measured.

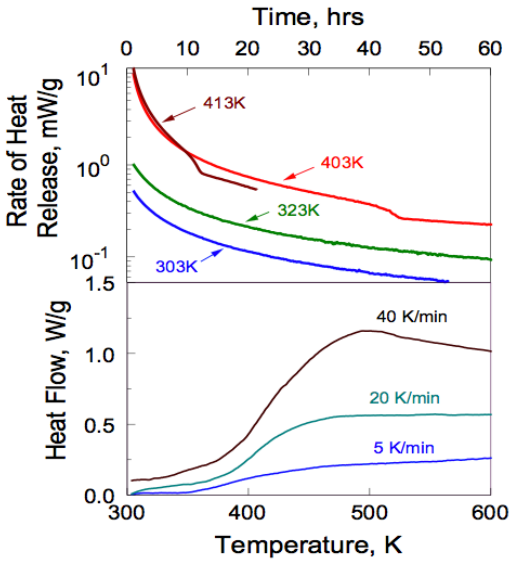

Figure 1: TAM III and DSC measurements of fully-dense nanocomposite Al·CuO powders. Upper plot: heat release rate, normalized by the sample mass, in the temperature interval 303–413 K. Lower plot: low temperature portions of DSC traces for fully-dense 2Al·3CuO nanocomposite powders measured at different heating rates [12].

Traces measured at 403 and 413 K, exhibit additional features compared to traces acquired at lower temperatures. Each high-temperature trace includes two stages with a relatively short transition period observed after about 10 and 40 hours for the samples reacting at 413 and 403 K, respectively. After the transition, the reaction rates decrease. Most likely, this transition is associated with a change in the structure of the growing interfacial Al2O3 layer, e.g., from amorphous to γ-crystalline, occurring when the layer grows above some critical thickness, specific for each temperature.

It was assumed that the initial parts of traces measured at 403 and 413 K are described by the same reaction mechanism as the measurements performed at 303 and 323 K. This reaction mechanism was also assumed to be active during early stages of the DSC experiments reported in ref [12]; the respective portions of the DSC signals are shown in Fig. 1. For all heating rates, a relatively sharp increase in the reaction rate was observed to occur between 350 and 450 K. As the temperature increased, the reaction rates stabilized or decreased at a higher heating rate.

MODEL AND DATA PROCESSING

Reaction kinetics model

The nanocomposite material was assumed to include mono-sized spherical CuO inclusions in Al matrix [8], see Fig. 2. Based on SEM images of particle cross-sections, inclusion diameters were taken as 100 nm. Reduction of CuO at relatively low temperatures often results in formation of metallic Cu, without formation of intermediate phases [18]:

$$3CuO + 2Al \rightarrow 3Cu + Al_2O_3 \quad (1)$$

Reaction (1) was considered in the model. The inclusion diameter was being corrected assuming that all Cu formed as a result of reaction (1) remained inside the inclusion. The CuO/Cu core was surrounded by a growing Al_2O_3 shell separating it from the Al matrix. The reaction rate is assumed to be limited by transport of reacting components through the shell.

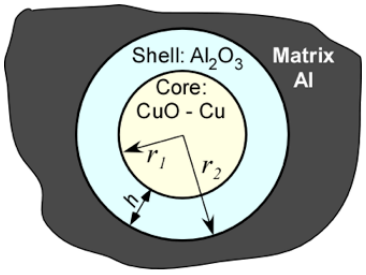

Figure 2: Core-shell geometry considered in the reaction model.

The rate of reaction was described by the CM model for the core-shell geometry [7, 8]:

$$\frac{dr_2}{dt} = K \exp\left(\frac{E_2}{k_B T}\frac{r_1}{r_2 h}\right) \quad (2)$$

where k_B is the Boltzmann constant, T is temperature, r_1 and r_2 are the radii of the CuO core and Al_2O_3 shell, respectively, h is the thickness of Al_2O_3 shell: $h=r_2-r_1$, and K is described by an Arrhenius expression with the activation energy E_1 and preexponent k_0:

$$K = k_0 \exp(-E_1 / RT) \quad (3)$$

The relation between radii, r_1, and r_2, is defined using a parameter $z = \frac{\sigma_{shell}}{\sigma_{core}}$, where σ_{core} and σ_{shell} are the respective volume changes of the core and shell [7, 8]:

$$r_2^3 - r_1^3 - \left(r_{20}^3 - r_{10}^3\right) = z\left(r_1^3 - r_{10}^3\right) \quad (4)$$

where r_{10} and r_{20} are the initial core and external shell radii, respectively.

The parameter E_2 of the CM model reflecting the effect of Mott potential on the rate of mass transfer may increase with temperature [19] as:

$$E_2(T) = a + bT \quad (5)$$

where a and b are constants.

Four unknown parameters were used in the model (1)-(5): k_0, E_1, a, b. They were found from joint processing of the results of DSC and TAM III measurements.

Data Processing

Both TAM III and DSC curves were interpreted to calculate changes in r_1 and h. The measured gravimetric rates of heat release, $\dot{q}_{exp}$, were first transferred into mass changes, m_i, for individual components in reaction (1):

$$\dot{q}_{\exp} = \frac{1}{M}\sum_i \Delta H_i \dot{m}_i \quad (6)$$

where subscript i stands for Al, Al_2O_3, CuO and Cu; ΔH_i is the specific enthalpy of formation of a respective component at the experimental temperature [20], and M is the total mass of material. Once the mass changes for individual components were calculated, the values of r_1 and h were found accounting for the component densities. For the time-dependent TAM III traces $\dot{q}_{exp}(t)$, the temporal changes in the radii $r_1(t)$, $r_2(t)$, and thickness h(t) were then inserted in the system of equations 2-5 to find the best fit values for K_0, E_1, a, and b. All traces were fitted simultaneously using a customized procedure [9]. This allowed the determination of the kinetic parameters shown in Table 1.

	Average	Range	
k_0, nm/s	2.1 x 10^{-3}	2.5 x 10^{-6}	1.8
E_1, J/mol	44000	28000	61000
E_2, 10^{-22} J-nm	-1502 + 5.52T	-2088 + 7.45T	-917+3.59T

Table 1: Kinetic parameters obtained from processing TAM III and DSC measurements.

RESULTS

Samples used in DSC experiments aged for several months. The aging time was estimated using the initial oxide thickness and kinetic parameters found. Values for the initial thicknesses of alumina shell h_0 found as adjustable parameters from fitting the DSC curves vary in the range of 0.77 – 1.04 nm.The freshly prepared samples were assumed to have h_0=0.39 nm [9].The time required to age such samples at room temperature to grow 0.77 and 1.04 nm-thick oxide layers were calculated to be 3 and 12 months, respectively. There is also good correlation between the calculated and measured DSC traces (Fig. 3). In particular, the calculated curves predict the observed increase followed by a relatively constant heat flow.

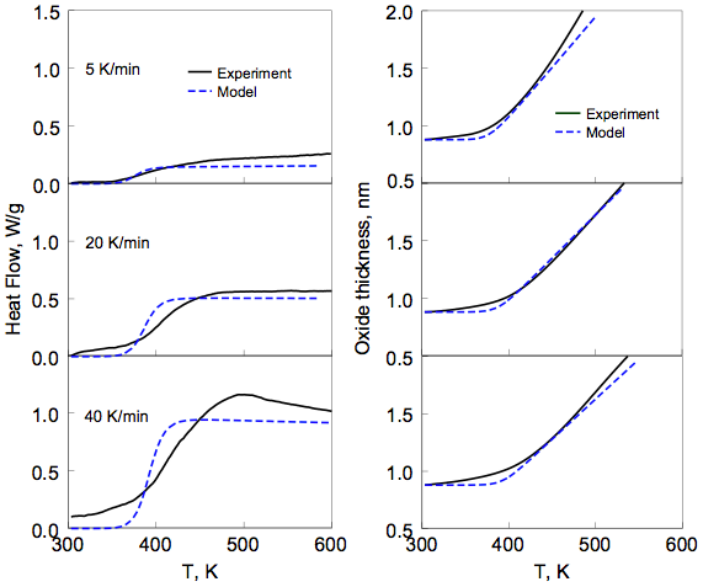

Figure 3: Experimental and theoretical DSC curves and oxide thickness at various heating rates. Initial thickness of Al_2O_3 at 303 K is 0.88 nm.

For TAM III traces shown in Fig. 4 (upper plot), experimental and calculated results overlap. Each TAM III trace starts with a specific h, while h_0=0.39 nm was used as a starting point for all calculations. The final result obtained in fitting the model to the DSC traces is shown in Fig. 4 (lower plot). The model couples a previously derived CM mechanism and an aluminum oxidation model including formation of different alumina polymorphs. The main features of the DSC curves are well described.

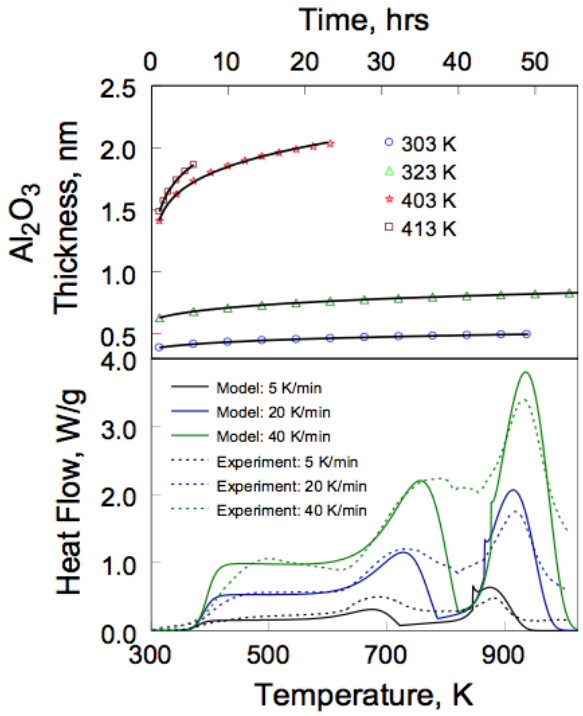

Figure 4: Upper plot: comparison of the alumina oxide thickness inferred directly from TAM III measurements (symbols) and that predicted using the identified reaction kinetics (lines). Lower plot: experimental and calculated DSC curves for 2Al•3CuO at heating rates of 5, 20, and 40 K/min.

CONCLUSION

Simultaneous processing of the experimental data from DSC and microcalorimetry enabled us to determine the parameters for the CM kinetics describing redox reaction in the ARM-prepared Al-CuO thermite.The parameters specified in Table 1 enable one to describe the initial portions of the DSC curves (up to 600 K) measured at different heating rates as well as microcalorimetry traces recorded in the temperature range of 303 – 413 K. Introduced reaction kinetics enables one to predict how such materials are aging. This model describes initial stages of thermal initiation of such reactive materials subjected to heating, including conditions with high heating rates experienced in many practical systems.The CM mechanism was successfully coupled with reaction kinetics describing processes occurring at higher temperatures, such as thermally activated diffusion-limited oxidation, polymorphic phase changes in the growing oxide layers, and consumption of oxygen from condensed phase oxidizers.

ACKNOWLEDGEMENT

This work was supported by US Army Research Lab and Defense Threat Reduction Agency.

REFERENCES

1. K. K. Kuo, G. A. Risha, B. J. Evans, E. Boyer, Mater. Res. Soc. Symp. Proc. 800 (2003) 3–14.

2. E. L. Dreizin. Energy Combust. Sci. 35 (2009) 141-167.

3. E. L. Dreizin, M. Schoenitz, Y.L. Shoshin, M. A. Trunov, Proc. 36th Int. ICT Conf./32nd Int. Pyrotech. Seminar, Karlsruhe, Germany, 2005, pp. 138/1-138/12.

4. E.L. Dreizin, M. Schoenitz, US Patent 7,524,355 B2 April 28, 2009.

5. M. Schoenitz, T.S. Ward, E. L. Dreizin, Mater. Res. Soc. Symp. Proc. 800 (2003) AA2.6.1-AA2.6.6.

6. M. Schoenitz, T.S. Ward, E.L. Dreizin, Proc. Combust. Inst. 30 (2005) 2071-2078.

7. Ermoline, A., and Dreizin, E.L. (2011). Chem. Phys. Let. 505, 47-50.

8. Ermoline, A., Schoenitz, M., and Dreizin, E.L. (2011). Combust. Flame 158, 1076-1083.

9. Ermoline, A., Stamatis, D., and Dreizin, E.L. (2012). Thermochim. Acta. 527, 52-58.

10. Stamatis, D., Ermoline, A., and Dreizin, E.L. (2012). Combust.Theor. Model. 16, 1011-1028.

11. M.A. Trunov, M. Schoenitz, E.L. Dreizin, Combust. Theor. Model. 10 (2006) 603-624.

12. S.M. Umbrajkar, M. Schoenitz, E.L. Dreizin, Thermochim. Acta 451 (2006) 34–43.

13. M. Schoenitz, S. Umbrajkar, E.L. Dreizin, J. Propul. Power 23 (2007) 683–687.

14. S.M. Umbrajkar, S. Seshadri, M. Schoenitz, V.K. Hoffmann, E.L. Dreizin, J. Propul. Power 24 (2008) 192–198.

15. N. Cabrera, N.F. Mott, Rep. Prog. Phys. 12 (1949) 163.

16. L.H.P. Jeurgens, W.G. Sloof, F.D. Tichelaar, E. Mittemejer, J. Appl. Phys. 92 (2002) 1649.

17. Q. Fu, T. Wagner, J. Phys. Chem. B 109 (2005) 11697-11705.

18. J.A. Rodriguez, , J.Y. Kim, , J.C. Hanson, M. Pérez, A.I. Frenkel, Catal. Lett. 85 (2003) 247-254.

19. F. Reichel, L.P.H. Jeurgens, E.J. Mittemeijer, Acta Mater. 56 (2008) 2897–2907.

20. http://webbook.nist.gov/chemistry/

For more information or to place an order, go to http://www.tainstruments.com/ to locate your local sales office information.